

RESEARCH PAPER

 OPEN ACCESS

## Linker flexibility of IVS3-S4 loops modulates voltage-dependent activation of L-type $\text{Ca}^{2+}$ channels

Nan Liu<sup>a</sup>, Yuxia Liu<sup>a</sup>, Yaxiong Yang<sup>a</sup>, and Xiaodong Liu<sup>a,b,c</sup>

<sup>a</sup>Department of Biomedical Engineering, School of Medicine, Tsinghua University, Beijing, China; <sup>b</sup>School of Life Sciences, Tsinghua University, Beijing, China; <sup>c</sup>IDG/McGovern Institute for Brain Research, Tsinghua University, Beijing, China

### ABSTRACT

Extracellular S3-S4 linkers of domain IV (IVS3-S4) of L-type  $\text{Ca}^{2+}$  channels ( $\text{Ca}_v1$ ) are subject to alternative splicing, resulting into distinct gating profiles serving for diverse physiological roles. However, it has remained elusive what would be the determining factor of IVS3-S4 effects on  $\text{Ca}_v1$  channels. In this study, we systematically compared IVS3-S4 variants from  $\text{Ca}_v1.1$ -1.4, and discover that the flexibility of the linker plays a prominent role in gating characteristics. Chimeric analysis and mutagenesis demonstrated that changes in half activation voltage ( $V_{1/2}$ ) or activation time constant ( $\tau$ ) are positively correlated with the numbers of flexible glycine residues within the linker. Moreover, antibodies that reduce IVS3-S4 flexibility negatively shifted  $V_{1/2}$ , emerging as a new category of  $\text{Ca}_v1$  enhancers. In summary, our results suggest that the flexibility or rigidity of IVS3-S4 linker underlies its modulations on  $\text{Ca}_v1$  activation ( $V_{1/2}$  and  $\tau$ ), paving the way to dissect the core mechanisms and to develop innovative perturbations pertaining to voltage-sensing S4 and its vicinities.

### ARTICLE HISTORY

Received 2 May 2016  
Revised 19 June 2016  
Accepted 23 June 2016

### KEYWORDS



L-type  $\text{Ca}^{2+}$  channels; linker flexibility; S3-S4 loop; voltage-dependent activation; voltage sensing domain

### Introduction


L-type  $\text{Ca}^{2+}$  channels (LTCCs), also named  $\text{Ca}_v1$  family, play a crucial role in numerous physiological functions by mediating  $\text{Ca}^{2+}$  influx, including muscle contraction, hormone secretion, gene transcription, synaptic transmission and cardiac pacemaking.<sup>1</sup> LTCC is formed as multimeric channel complex, by auxiliary subunits such as  $\beta$  and  $\alpha_2\delta$ , and the prominent pore-forming  $\alpha_1$  subunit, composed of 4 homologous but non-identical domains, each of which contains a series of 6 transmembrane  $\alpha$ -helical segments, numbered S1–S6, which are linked by both intracellular and extracellular loops.<sup>2,3</sup> Segments S1-S4 form voltage sensing domains (VSDs), and segments S5-S6 constitute the permeation pore.<sup>2</sup> VSDs could act as transducers of transmembrane voltage potentials by positively charged S4, leading to subsequent conformational changes.<sup>4,5</sup>

The extracellular loops linking S3 and S4 (S3-S4 loops or linkers) may influence the function of VSDs

presumably by controlling the downstream molecular interactions, *e.g.*, between S3 and S4.<sup>6–10</sup> It has been reported that certain subtypes of  $\text{Ca}_v$  channels, including  $\text{Ca}_v1.1$ ,  $\text{Ca}_v1.2$ ,  $\text{Ca}_v2.1$  and  $\text{Ca}_v2.2$  channels, are subject to alternative splicing of short exons within the S3-S4 loops of domain IV (IVS3-S4). These splice variants exhibit distinct gating characteristics, particularly the voltage-dependent activation, implying an important role of IVS3-S4 in VSD behaviors thus the channel gating.<sup>7,11–15</sup> However, it is still unclear about the determining factor underlying differential modulations by diverse variants of the linker. Such determinant is potentially shared as common principles to different subtypes and variants across the LTCC family. It would be intriguing and beneficial to systematically compare all the family members, *i.e.*,  $\text{Ca}_v1.1$ –1.4, in the context of IVS3-S4 modulations and mechanisms. First, IVS3-S4 of natural variants would be properly and quantitatively evaluated for its effects on gating,

**CONTACT** Xiaodong Liu  [liuxiaodong@tsinghua.edu.cn](mailto:liuxiaodong@tsinghua.edu.cn)  Biomedical Engineering, School of Medicine, Tsinghua University, B307 Med. Sci. Bldg., Beijing 100084, China.

Color versions of one or more of the figures in this article can be found online at [www.tandfonline.com/kchl](http://www.tandfonline.com/kchl).

 Supplemental data for this article can be accessed on the [publisher's website](#).

© 2017 Nan Liu, Yuxia Liu, Yaxiong Yang, and Xiaodong Liu. Published with license by Taylor & Francis.

This is an Open Access article distributed under the terms of the Creative Commons Attribution-Non-Commercial License (<http://creativecommons.org/licenses/by-nc/3.0/>), which permits unrestricted non-commercial use, distribution, and reproduction in any medium, provided the original work is properly cited. The moral rights of the named author(s) have been asserted.

which are supposedly in part responsible for different gating profiles of  $\text{Ca}_v1$  subtypes. Sporadic evidence on the IVS3-S4 effects has been reported, such as from  $\text{Ca}_v1.1$  and  $\text{Ca}_v1.2$ , but it is imperative to extend to the whole  $\text{Ca}_v1$  family. Second, the mechanisms of IVS3-S4 would help provide further insights into the working principles of VSDs and channel activations of  $\text{Ca}_v1$  channels. Understanding toward voltage-dependent activation specific to  $\text{Ca}_v1$  channels has been limited thus far.<sup>2,7,16</sup> Third, new strategies could be devised to modulate  $\text{Ca}_v1$  channels for potential therapeutics, e.g., small molecules or antibodies, by targeting and perturbing the key activation mechanism related to the IVS3-S4 loops.

In this study, we systematically examined and compared IVS3-S4 linkers across LTCCs, which contain the exons with different abundance of glycine residues ( $G_X$  linkers). Further analysis by chimeric channels, mutagenesis and specific antibodies suggest that the flexibility of  $G_X$  linker would be the major index to determine the mobility of VSD thus the potency of modulatory effects on  $\text{Ca}_v1$  activation.

## Results

### ***IVS3-S4 loops from $\text{Ca}_v1$ channel family differentially modulate voltage-dependent activation***

In LTCCs, 4 pore-forming  $\alpha_1$  subunit isoforms ( $\alpha_{1S}$ ,  $\alpha_{1C}$ ,  $\alpha_{1D}$  and  $\alpha_{1F}$ ) exhibit distinct biophysical properties and expression profiles, to accommodate different cellular-specific or tissue-specific needs.<sup>11,12,17-21</sup> The IVS3-S4 loop of all  $\alpha_1$  subunits contains the splicing exon: exon 29 in the skeletal muscle  $\text{Ca}_v1.1$  channel, exon 33 in the cardiac  $\text{Ca}_v1.2$  channel, exon 32 in the neuronal  $\text{Ca}_v1.3$  channel, and exon 32 in the retinal  $\text{Ca}_v1.4$  channel (Fig. 1A). The coding sequences of these exons (yellow colored) appear to differ in the length and also in the number of glycines (red colored). To examine the role of various IVS3-S4 loops in voltage-dependent activation, we constructed  $\text{Ca}_v1.3$  chimeric channels by inserting corresponding exons from the 4  $\alpha_1$  subunits into a natural splice variant of  $\alpha_{1D}E32_{1D\Delta}$  (lacking exon  $E32_{1D}$ ), which has rather short linker and decent current in HEK cells. In response to membrane potentials ( $V_m$ ) of the step protocol, current traces color-coded for  $V_m$  of  $-30$  mV,  $-10$  mV and  $+10$  mV indicated significant differences in channel activation between  $\alpha_{1D}E32_{1D\Delta}$  control and chimeric channels (Fig. 1B). For

both rows of current traces, in accordance with longer exons/linkers, less activation could be achieved at particular  $V_m$ , indicated by the traces appearing at lower positions for  $-30$  mV step (blue traces). As quantified by half-activation voltage ( $V_{1/2}$ ) values, the activation curves were significantly shifted to the positive direction by the linkers (Fig. 1C). Apparently the length of the linker plays an important role in the modulation of channel activation, as suggested by the comparison between  $\alpha_{1D}E32_{1D\Delta}$  and  $\alpha_{1D}E29_{1S}$ , the latter of which has the longest linker and also the most significant  $V_{1/2}$  shift ( $\Delta V_{1/2}$ ) (Fig. 1D). The positive shift of  $\alpha_{1D}E32_{1F}$  activation as compared with  $\alpha_{1D}E32_{1D\Delta}$  can also be explained by their difference in the linker length. However, we noticed that although  $E32_{1F}$  is the shortest exon, the  $E32_{1F}$  linker also produced a significant  $\Delta V_{1/2}$ , just second to that of  $E29_{1S}$ . Closer examinations suggested that the richness of glycines within the linker could also play a prominent role, which led us to hypothesize that the flexibility of linkers modulates the activation of  $\text{Ca}_v1$  channels.

### ***Enrichment of glycines within IVS3-S4 loops further attenuates voltage-dependent activation***

To test the flexibility hypothesis, we gradually substituted original amino acids of exons  $E32_{1F}$  and  $E29_{1S}$  with glycines, achieving mutant channels containing different numbers of glycines:  $G_3$ ,  $G_4$  and  $G_7$ ; and  $G_6$ ,  $G_{10}$  and  $G_{19}$ , based on  $\alpha_{1D}E32_{1F}$  and  $\alpha_{1D}E29_{1S}$  respectively (Fig. 2A). Glycine enrichment of IVS3-S4 loops further positively shifted the activation of the channels with more positive  $V_{1/2}$ , evidenced from their exemplar traces before and after full glycine substitutions (Fig. 2B). Moreover, gradual changes of  $V_{1/2}$  can be observed from both groups of  $\alpha_{1D}E32_{1F}$  and  $\alpha_{1D}E29_{1S}$  channels, indicating an apparent trend of  $V_{1/2}$  modulations in accordance to the number of glycines (Fig. 2C). Glycines add more flexibility to the motif in the protein structure.<sup>22</sup> We reason that the glycine-mediated flexibility may be the more direct factor underlying the voltage-dependent activation of channel variants containing different linkers.

### ***Positive correlations between the flexibility of $G_X$ linkers and the activation characteristics of $V_{1/2}$ and $\tau$***

Collecting up all channel variants with different IVS3-S4 loops, our results show  $V_{1/2}$  values of the mutant

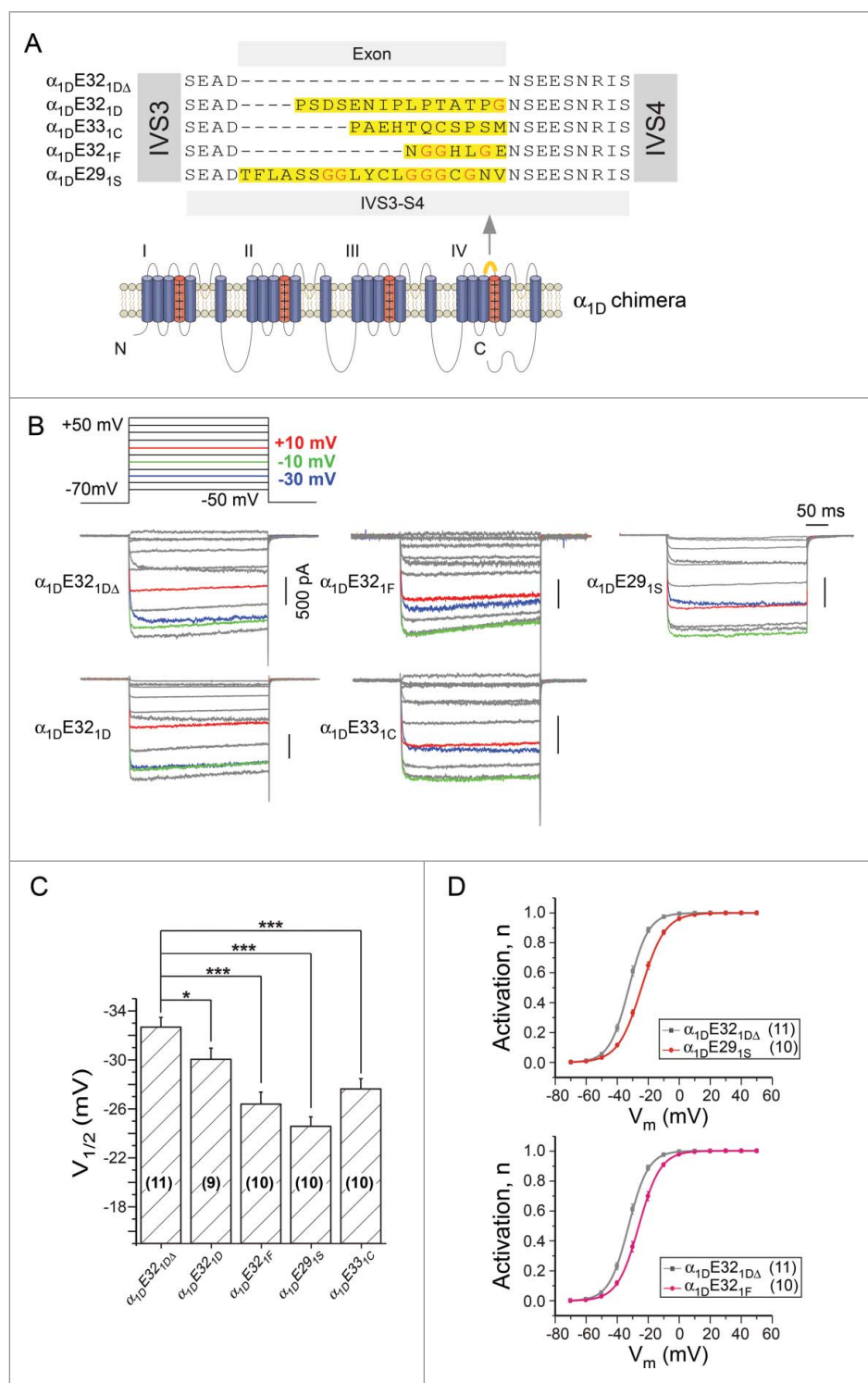


**Figure 1.** Comparison among different IVS3-S4 variants from  $Ca_v1$  family. (A) Construction scheme for  $\alpha_{1D}$  chimeras targeting the splicing exon. Based on 2 natural splice variants of exon32:  $\alpha_{1D}E32_{1D\Delta}$  and  $\alpha_{1D}E32_{1D}$ , additional chimeric channels were constructed with  $\alpha_{1D}E32_{1D\Delta}$  as the backbone inserted into E32-equivalent exons from  $\alpha_{1S}$ ,  $\alpha_{1F}$  and  $\alpha_{1C}$ , respectively. E32 or E32-equivalent exons are highlighted as yellow in both the sequence alignment and the cartoon of  $\alpha_{1D}$  topology. Glycine residues are marked in red. (B) Modulations of voltage-dependent activation of  $\alpha_{1D}$ -based chimeric channels. The voltage protocol was composed of 10 mV steps ranging from  $-50$  mV to  $+50$  mV. Representative whole-cell  $Ba^{2+}$  currents were from HEK293T cells expressing  $\alpha_{1D}$  chimeras, with traces at  $-30$  mV,  $-10$  mV and  $+10$  mV colored as shown. (C) Comparison of  $V_{1/2}$  values (voltage at 50% activation, n) between  $\alpha_{1D}E32_{1D\Delta}$  and  $\alpha_{1D}$  chimeras of  $\alpha_{1D}E32_{1F}$ ,  $\alpha_{1D}E29_{1S}$ , and  $\alpha_{1D}E33_{1C}$  respectively. \*,  $p < 0.05$  and \*\*\*,  $p < 0.001$ . (D) Voltage dependence of channel activation of  $\alpha_{1D}E29_{1S}$ , or  $\alpha_{1D}E32_{1F}$  compared with that of  $\alpha_{1D}E32_{1D\Delta}$ .

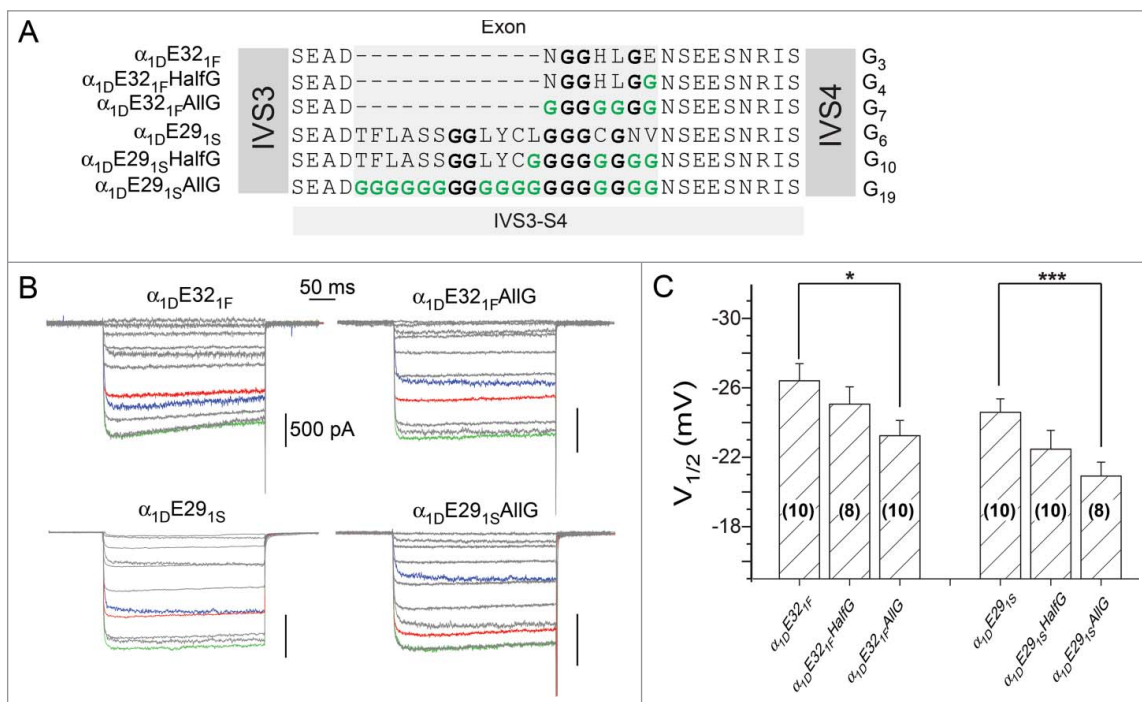


**Figure 2.** The strategy to change the flexibility of IVS3-S4 linkers by enrichment of glycine residues. (A) The summary of point mutations to glycine residues. Based on chimeric channels of  $\alpha_{1D}E32_{1F}$  and  $\alpha_{1D}E29_{1S}$  containing native variants of IVS3-S4, glycine (G) residues gradually replaced the original sites of amino acids for each chimera. According to the percentage of glycine residues, the constructs are named as HalfG or AllG. (B) Exemplar current traces of selected mutant channels in (A), in response to the same voltage protocols and the color scheme as in Figure 1B. Top row and bottom row are based on  $\alpha_{1D}E32_{1F}$  and  $\alpha_{1D}E29_{1S}$ , respectively. According to the number of glycine residues ( $G_x$ ), for top row from the left to right,  $X = 3$  or  $7$ ; and  $X = 6$  or  $19$  for the bottom row. The statistics of the group data is shown in (C), with the number of cells indicated for each chimera. \*,  $p < 0.05$  and \*\*\*,  $p < 0.001$ .

channels became more positive with the number of glycine residues being increased (Fig. 3A). The shift in  $V_{1/2}$  was accompanied by the change in slope factor (S):  $3.0 \pm 0.2$  ( $n = 11$ ) for variant  $G_0$  and  $3.6 \pm 0.1$  ( $n = 11$ ) for variant  $G_{19}$ ,  $p < 0.01$ . This is within expectations as both  $V_{1/2}$  and S could be the manifestation of decreased apparent sensitivity to  $V_m$  along with increased number of glycines. Meanwhile, either insertion of native alternative splicing exons or enrichment of glycine residues slowed down the activation kinetics of the channel (Fig. 3B). In addition, the statistic results demonstrate that the number of glycines within IVS3-S4 loop is positively correlated with  $V_{1/2}$  and the time constant ( $\tau$ ) of the channel (Fig. 3C and D), confirming the flexibility of IVS3-S4 loop provided by glycine residues can significantly impair the activation of Cav1.3 channels.

#### **Antibodies that bind and constrain IVS3-S4 enhance channel activation by negative $\Delta V_{1/2}$**

Inspired by prior report that antibodies binding onto extracellular loops could act as innovative channel

modulators,<sup>23</sup> we devised a similar strategy to target the IVS3-S4 linker based on our findings here, in hope to specifically modulate channel activation. As the proof of concept, we first inserted the His-tag (6 histidine residues) into IVS3-S4 loop of  $\alpha_{1D}E32_{1D\Delta}$  to construct  $\alpha_{1D}E32_{1D\Delta}6His$ , which would be recognized and bound by antibodies of Anti-His-tag right at the loop of IVS3-S4. TIRF imaging confirmed that only cells expressed with  $\alpha_{1D}E32_{1D\Delta}6His$  channels, but not control cells, can be recognized by the antibody (Fig. 4A). As expected, the activation of  $\alpha_{1D}E32_{1D\Delta}6His$  channels was significantly shifted to the left after incubating with Anti-His-tag, as evidenced by the exemplar traces (Fig. 4B) and the statistical analysis of the activation curves (Fig. 4C). Supposedly, the antibody constrains the flexibility of the loop, thus limits the randomized mobility of VSD, which would counteract with the rightward activation shift due to the flexible linker. As further assurance of our design, the effect of Anti-His-tag did not cause any significant shift of  $V_{1/2}$ , for control channels ( $\alpha_{1D}E32_{1D\Delta}$  without His-tag,  $p > 0.6$ ) or under control conditions (intracellular application of Anti-His-tag,  $p > 0.5$ ). In addition, we also performed another set of experiments based on the



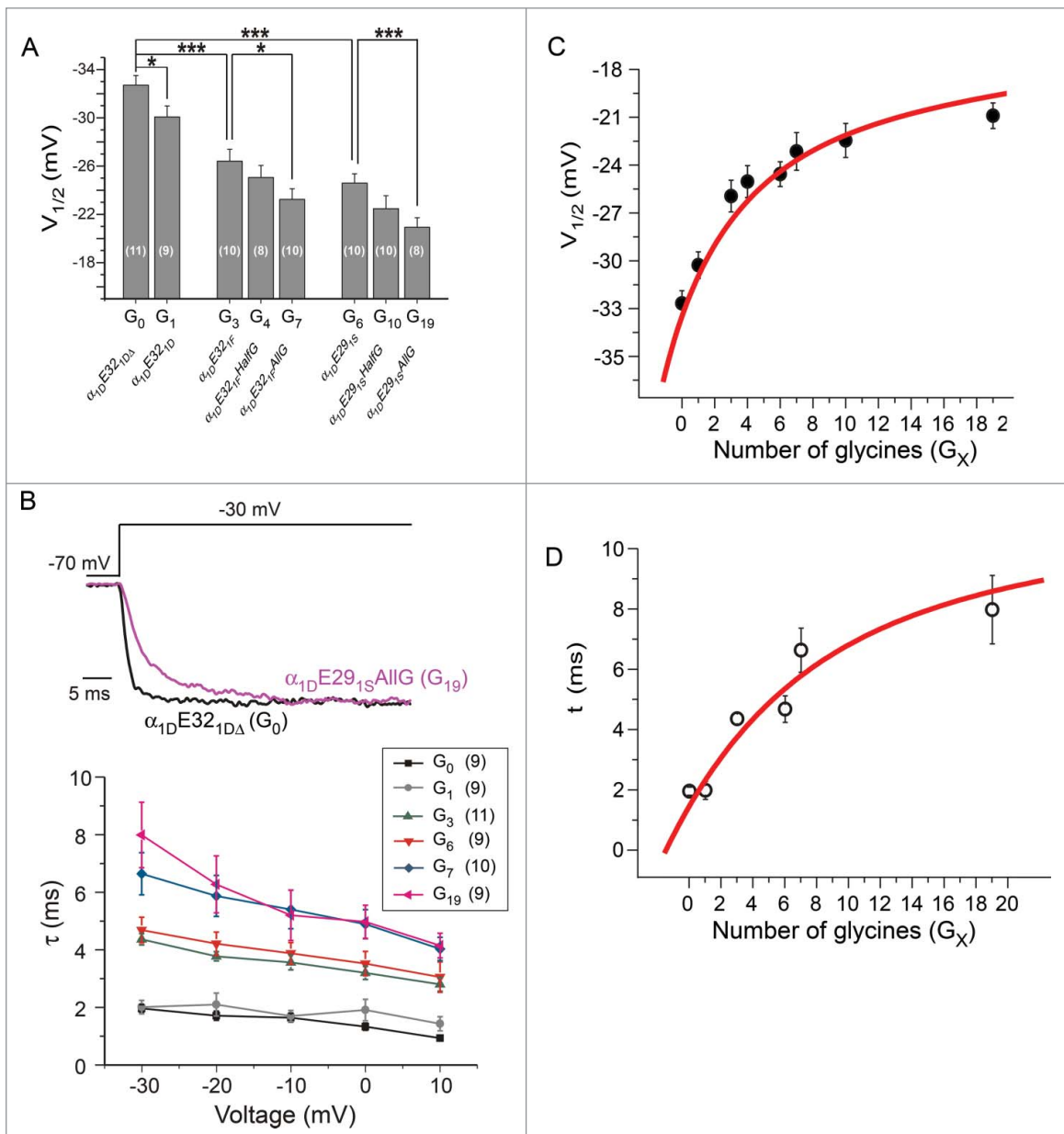


**Figure 3.** Effects of IVS3-S4 on  $Ca_v1.3$  activation are correlated with the number of glycine residues of the linker. (A) Summary of  $V_{1/2}$  for various  $\alpha_{1D}$  channels including the native forms and chimeric mutants. These channel constructs were also named according to the number of glycines ( $G_X$ ) within the linker. \*,  $p < 0.05$  and \*\*\*,  $p < 0.001$ . (B) Flexibility of different  $G_X$  linkers affected the kinetics of channel activation. At  $-30$  mV, time constant ( $\tau$ ) values of current traces were fitted, as shown by the exemplars of  $G_0$  and  $G_{19}$  (upper), and summarized for voltages from  $-30$  mV to  $+10$  mV (lower). (C and D) Correlations between the linker flexibility ( $G_X$ ) and voltage-dependence ( $V_{1/2}$ ) or time-dependence ( $\tau$ , at  $-30$  mV) of activation. The red lines are visually appended to illustrate the trends in relation to  $G_X$  and loop flexibility.

channel variant with  $G_{19}$  linker, which confirmed the antibody effects of activation enhancement (Fig. S1).

#### Effects on channel activation arising from IVS3-S4 and C-terminus are additive

We next explored another established modulation of channel gating mediated by the competition between

distal carboxyl terminus (DCT) and apo-calmodulin ( $Ca^{2+}$ -free CaM)<sup>16,24</sup> (Fig. 5A). One major phenotype according to the modulation profiles is the shift of activation: DCT such as DCT<sub>F</sub> (strong DCT from  $\alpha_{1F}$ ) would positively shift  $V_{1/2}$  whereas CaM would leftward shift  $V_{1/2}$ . Although the detailed mechanism about how CaM pre-associated channel affects the gating is unclear, a reasonable assumption is that channels fully bound with

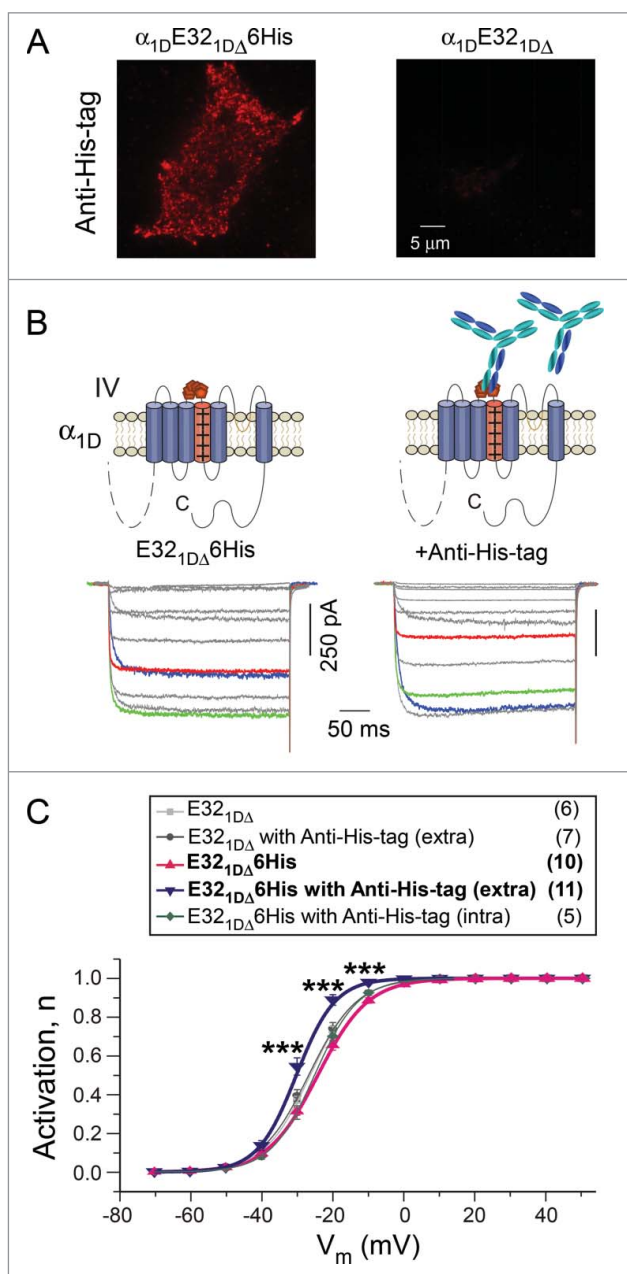


**Figure 4.** Antibody targeting IVS3-S4 loop modulated the activation of channels. (A) His-tag antibodies (Anti-His-tag) recognized  $\alpha_{1D}E32_{1D\Delta}6His$  on the cell membrane, compared with  $\alpha_{1D}E32_{1D\Delta}$  as the control group. (B) Exemplar current traces of the  $\alpha_{1D}E32_{1D\Delta}6His$  channels without/with extracellular incubation (ex) of Anti-His-tag antibodies. The voltage protocol and color scheme are the same as in Figure 1B. (C) Voltage dependence of the activation curves. A significant leftward shift in  $\alpha_{1D}E32_{1D\Delta}6His$  activation was evidenced without/with His-tag antibodies in the extracellular solution (extra), as indicated by the differences in the level of activation at particular voltages (\*\*\*,  $p < 0.001$ ). No difference existed among channels of  $E32_{1D\Delta}$ ,  $E32_{1D\Delta}$  with antibodies extracellularly applied (extra),  $E32_{1D\Delta}6His$ , or  $E32_{1D\Delta}6His$  with antibodies intracellularly applied through pipettes (intra).

CaM reach the maximum activation (most negative  $V_{1/2}$ ); in parallel, every DCT-bound channel such as  $\alpha_{1D\Delta}DCT_F$  is essentially CaM-less thus approaching the most positive  $V_{1/2}$  (rightward shifted). We were asking about the potential relationship between these 2 types of modulation:  $G_X$  and CaM.  $DCT_F$  caused additional shift of  $V_{1/2}$  for channels with either short ( $G_0$ ) or long ( $G_{19}$ ) linkers (Fig. 5B and C). From the perspective of  $G_X$  effects, increasing number of glycines (enriched  $G_X$ , from  $G_0$  to  $G_{19}$ ) produced further rightward shift for channels with (CaM+) or without (CaM-) pre-associated CaM. Alternative interpretations would be: for CaM- channels,  $G_X$  changing from  $G_0$  to  $G_{19}$  made the channel even more difficult to open as compared with the  $V_{1/2}$  limit of “CaM-” channels; on the other hand, for CaM+ channels,  $G_X$  changing from  $G_{19}$  to  $G_0$  negatively shifts the channel beyond the  $V_{1/2}$  limit of “ $G_{19}$  CaM+” channels (Fig. 5D). The latter view emphasizes the additive nature of IVS3-S4 and CaM effects, strongly suggesting that the 2 mechanisms should follow different (non-overlapped) downstreams in modulation of  $Ca_v1$  activation.

## Discussion

This study focuses on the mechanism of action underlying the modulation of IVS3-S4 loop on voltage-dependent gating and provides the evidence to support the flexibility of IVS3-S4 loop as the major factor.

### Implications on physiological roles of IVS3-S4 variants of $Ca_v$ channels

Several earlier studies reported that S3-S4 loops of voltage-gated ion channels have significant impact on voltage dependence and temporal kinetics of activation.<sup>11-15,17,25</sup> In both P/Q-type  $Ca_v2.1$  and N-type  $Ca_v2.2$  channels, alternatively spliced exons 31a contain only 6 nucleic acid bases, encoding NP or ET at IVS3-S4 loop, respectively. The presence of NP or ET causes slower activation kinetics for both channels,<sup>13-15</sup> but with preferential distributions: NP of  $Ca_v2.1$  in the central nervous system,<sup>15</sup> and ET of  $Ca_v2.2$  in the peripheral,<sup>13</sup> suggesting specific neurons may utilize IVS3-S4 loop as one of the sophisticated mechanisms to gauge channel gating and  $Ca^{2+}$  signaling.

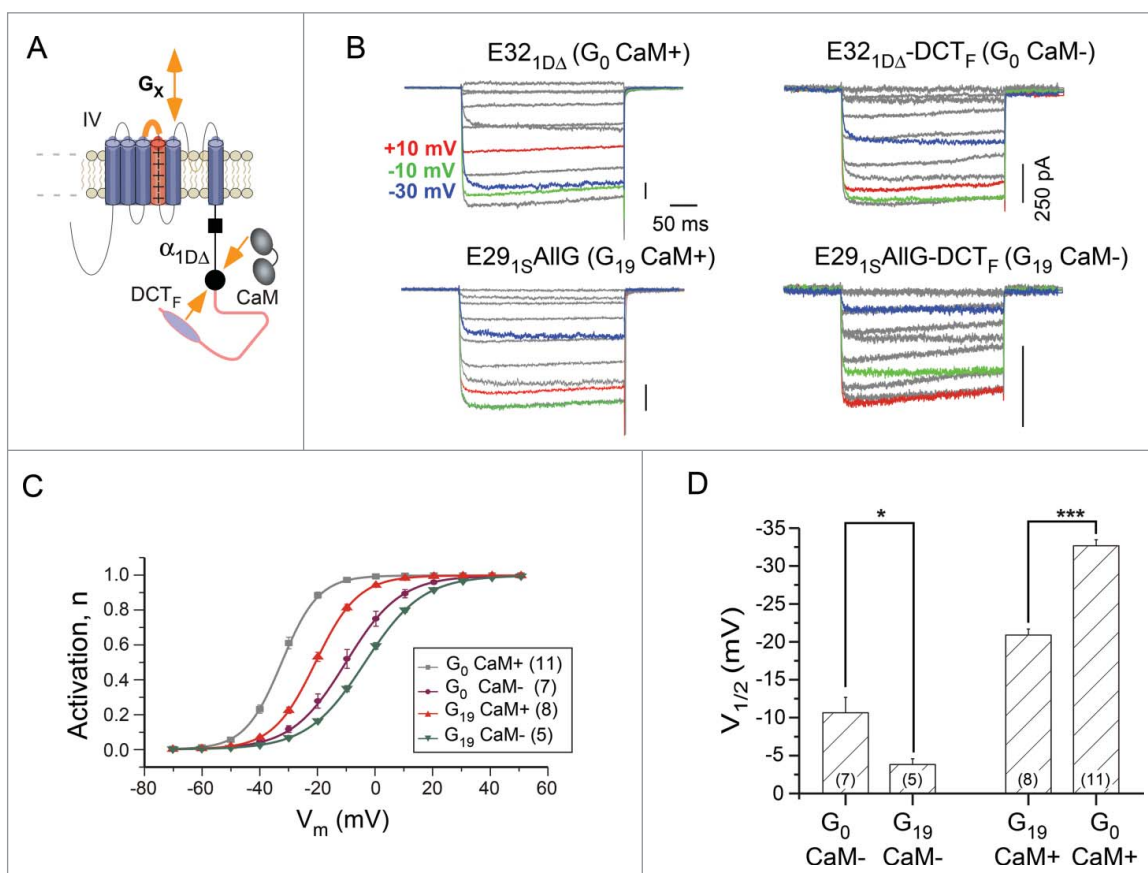


**Figure 5.** The additive effects on channel activation due to the flexible IVS3-S4 linker and DCT/CaM competition. (A) Two different mechanisms that modulate the voltage-dependent activation of  $Ca_v1.3$  channels. In addition to the IVS3-S4 linker where the flexibility presumably modulates the function of VSD,  $Ca_v1.3$  channels are also subject to the competitive tuning between DCT and CaM for which the channel activation is dependent on whether CaM is preassociated with the channel. Both  $G_x$  linker (increasing flexibility) and competitive DCT (kicking-off apoCaM) would cause the positive shift of channel activation. (B and C) Exemplar traces for different combinations of  $G_x$  and DCT effects. The native form of  $\alpha_{1D}E32_{1D\Delta}$  ( $G_0$  CaM+) contains a DCT motif with much weaker strength in competition with CaM than DCT from  $\alpha_{1F}$  (DCT<sub>F</sub>).  $E29_{1S}AllG$  consists of the linker from exon 29 of  $\alpha_{1S}$  but with glycine substitutions ( $G_{19}$  CaM+).  $\alpha_{1D}E32_{1D\Delta}-DCT_F$  ( $G_0$  CaM-) is the chimeric channel fused with DCT<sub>F</sub> to  $\alpha_{1D}$ , essentially replacing the DCT of the native form in  $\alpha_{1D}E32_{1D\Delta}$  ( $G_0$  CaM+).  $\alpha_{1D}E29_{1S}AllG-DCT_F$  ( $G_{19}$  CaM-) is to incorporate DCT<sub>F</sub> while containing the  $G_{19}$  linker within the loop. Experimental conditions and color schemes are similar to Figure 1B. (C and D) Comparison among the voltage dependence of the activation curves, for the 4 kinds of channels under tests. Activation curves (C) and statistics of  $V_{1/2}$  values (D) are shown for each channel subtypes. \*,  $p < 0.05$ ; \*\*\*,  $p < 0.001$ .

For  $Ca_v1.1$  and  $Ca_v1.2$  of LTCCs, different IVS3-S4 spliced variants also exist distinct distributions, suggesting LTCCs may also take advantage of IVS3-S4 to alter channel activities to control  $Ca^{2+}$  signals. In  $Ca_v1.1$  channel, the variant lacking exon 29 is distributed at low levels in differentiated muscle, but abundantly expressed in myotubules, and this variant shows a significant left-shifted  $V_{1/2}$  and a substantially increased current density.<sup>17</sup> For  $Ca_v1.2$  channels, IVS3-S4 splice variants display different levels of expression in fetal and adult heart and brain, and all the IVS3-S4 variants demonstrate unmistakable  $V_{1/2}$  shifts.<sup>12</sup>  $Ca_v1.3$  splice variants exhibit distinct percentages of abundance in brain and neuroendocrine

cells.<sup>20</sup> For  $Ca_v1.4$ , splice variants are distributed not only in retina but also in the immune system.<sup>21</sup>

### Systematic comparison across the whole $Ca_v1$ family

$Ca_v1.3$  and  $Ca_v1.4$  channels are also subject to alternative splicing within IVS3-S4 loop, however, the gating modulation of this loop is lacking.<sup>19,20</sup> In this work, we devised the chimeric analysis to symmetrically evaluate the functional roles of splicing exons within IVS3-S4 loops from the entire LTCC family. Results confirmed the previous observation of inhibitory effects on the channel activation, including positive  $V_{1/2}$  shift (Fig. 1), slower activation  $\tau$  (Fig. 3), etc.,

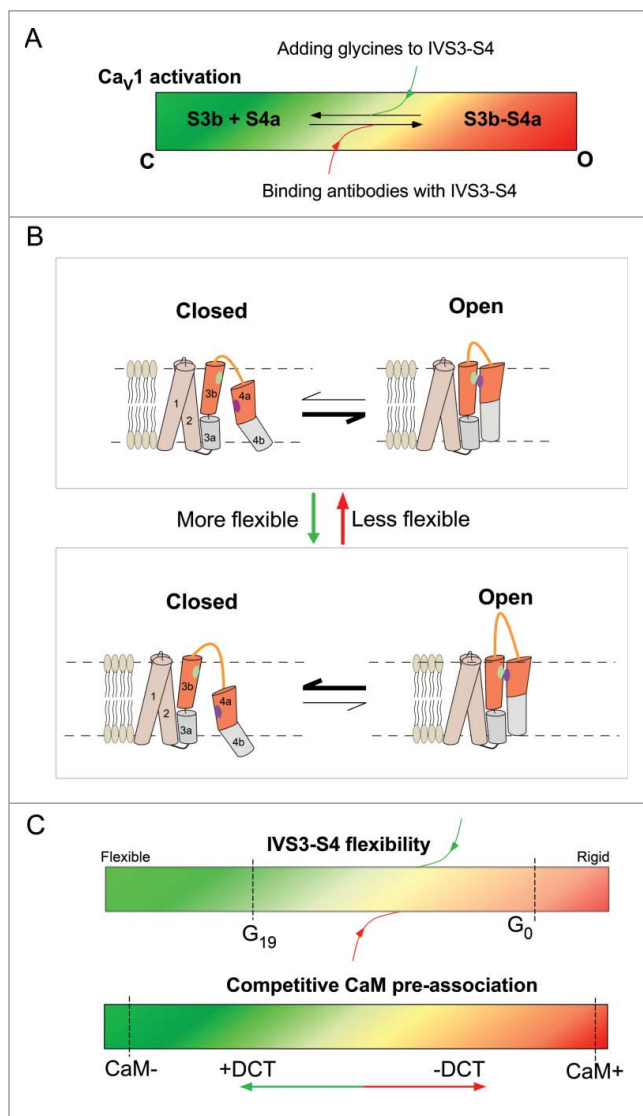


**Figure 6.** Schematic summary of IVS3-S4 modulation on  $\text{Ca}_v1$  activation. (A) Scheme of summary. Channel activation can be considered being controlled by the cooperative behaviors (binding and downstream events) between S3 and S4.  $G_X$  linkers attenuate whereas loop-bound antibodies facilitate the activation. The color codes (green, closed; red, open) are to indicate the open probability or the fraction of open channels. (B) Cartoons to illustrate the potential mechanism of flexibility-mediated channel gating. Increasing flexibility of VSD movement would reduce the chance of appropriate VSD positioning for the key sites to interact (indicating by green and violet dots); and decreasing the random movement of VSD would do the opposite. (C) The summary and comparison for the 2 major kinds of modulation in this study. The dynamic range and perturbations related to IVS3-S4 (upper) and CaM (lower) are compared. Color codes are in similar fashion to (A).

but extended onto the whole  $\text{Ca}_v1$  family. Also, the order of modulation strength as demonstrated by chimeric analysis is  $\text{E29}_{1\text{S}} > \text{E32}_{1\text{F}} > \text{E33}_{1\text{C}} > \text{E32}_{1\text{D}}$ , consistent with the activation profiles of  $\text{Ca}_v1$

channels following the same order:  $\text{Ca}_v1.1 > \text{Ca}_v1.4 > \text{Ca}_v1.2 > \text{Ca}_v1.3$ ,<sup>10,16,20,25</sup> where  $\text{Ca}_v1.1$  is the most hard-to-activate  $\text{Ca}_v1$  and  $\text{Ca}_v1.3$  has the most negative  $V_{1/2}$  (Fig. S2).

### Mechanistic insights into the effects by IVS3-S4 loops

Regarding the mechanisms underlying IVS3-S4 modulation, it has been speculated that the length of the linker might be the key factor,<sup>12</sup> which also appears to be consistent with our data. However, more thorough comparison and mutagenesis suggest that the flexibility of the loop would be the more direct index. Other properties, such as hydrophobicity, of the linker peptide might also underlie the  $G_X$  modulation. So we examined the hydrophobicity of  $\text{E32}_{1\text{F}}$  and  $\text{E29}_{1\text{S}}$ , and both linkers turn out to be neutral peptides; when the residues are completely replaced with glycines (low hydrophobic index, so producing neutral peptides), the richness of glycines strongly modulates the channel function ( $G_7$  and  $G_{19}$ ) while the overall hydrophobicity remains unaltered. Thus, it is unlikely that hydrophobicity plays any significant role in the  $G_X$  effects in this work. Whether under certain circumstances the hydrophobicity of the linker could also cause appreciable effects on channel function, as an intriguing perspective, inviting future investigations.

The consensus has been reached that upon depolarization S4 should move to appropriate position (e.g., to interact with S3) and activate the channel (Fig. 6A and B). Meanwhile, S4 as part of the VSDs is also dynamic and subject to random movement which could be highly regulated by the flexible linker of IVS3-S4. It is unlikely that the  $G_X$  linker directly interferes with the voltage-dependent VSD movement, but instead, adding glycines further randomizes VSD dynamics, reducing the chance for S3-S4 cooperation, under the conditions of both with and without depolarization. In this context, regardless of the actual perturbations, which could be the length or the number of glycines being increased, the same consequence would be caused: the flexibility of VSD is increased, so is the randomness of the movement, eventually the channel would end up with lower open probability at different  $V_m$ , i.e., more positive  $V_{1/2}$  or less activation (Fig. 6B). In this view, the degree of freedom in VSD movement (i.e., the number of glycines) would determine the effective concentration for the interaction,<sup>22</sup> or in an alternative



view the probability of S4 to appear in appropriate positions favoring the S3-S4 cooperation or interaction<sup>7</sup>. In this context, our study and related work from other groups are complementary to each other: we focus on changes in effective concentrations of the interacting peptides and they emphasize on changes in binding affinity between S3 and S4 motifs<sup>7,10</sup>, altogether supporting such putative reaction-based scheme we proposed (Fig. 6B).

Also, applying depolarization or attaching antibody can provide confinement to VSD dynamics, reducing the space of random walk, effectively promoting the probability of S3-S4 binding, as one way to understand the mechanism of voltage-dependent activation. In this work, we explored the dynamic range of the modulation by  $G_X$ -linker, by chimeric channels, mutagenesis and loop-specific antibodies, which are supposed to be extendable (Fig. 6C, upper panel). In contrast, prior works assure that CaM+ and CaM- channels, if not reaching, are very closely approaching the limits of the dynamic range set by DCT/CaM modulation (Fig. 6C, lower panel). This led us to realize that the loop flexibility is unlikely overlapped with the activation mechanism mediated by CaM modulation, since further  $V_{1/2}$  shifts arising from  $G_X$ -modulation on CaM+ (from  $G_{19}$  to  $G_0$ ) or CaM- (from  $G_0$  to  $G_{19}$ ) channels were substantially extended beyond the limits of DCT/CaM modulation.

We in this study rely on the analysis of voltage-dependence ( $V_{1/2}$  and  $S$ ) and temporal-kinetics ( $\tau$ ), which are the 2 most prominent aspects of channel activation. Regarding other channel characteristics, current density should be modulated by  $G_X$ -linkers as well, presumably similar to  $V_{1/2}$  and  $\tau$  (e.g., higher current density corresponding to facilitated channel activation), in consistence with our observations and other published reports;<sup>7</sup> whereas CDI (Ca<sup>2+</sup>-dependent inactivation) did not have any appreciable change with  $G_X$ -linker modulation (Fig. S3).

### **Proof of concept to inspire strategies of developing innovative Ca<sub>v</sub>1 modulators**

Our work demonstrates the potentials to devise more potent perturbations, including longer  $G_X$ -linkers and corresponding antibodies, both of which would exhibit broader range of activation tuning in both directions ( $\Delta V_{1/2}$ ,  $\Delta\tau$ , etc.). Extracellular loop might be an intriguing target to develop specific antibody-

based modulators for both research and therapeutic purposes.<sup>23</sup> Our success in applying antibodies targeting IVS3-S4 to modulate Ca<sub>v</sub>1 activation, as a proof of principle, opens up the avenue to explore the potentials of such Ca<sub>v</sub>1 openers or enhancers with new mechanism of action. It is worth to further develop more potent (by optimizing antibody properties) and more applicable (by producing antibodies specific to the native loops) antibody-based modulators. Also, we provide the evidence that the facilitation of activation due to CaM<sup>16</sup> can be utilized as an additive modulation in parallel with IVS3-S4 effects, altogether would provide much broader space of potency than any strategy currently known. By such “cocktails” of Ca<sub>v</sub>1 inhibition or facilitation combining the effects from both loop flexibility and apoCaM,  $\Delta V_{1/2}$  could reach up to  $-30$  mV or more, as estimated from our data (Fig. 5D).

## **Materials and methods**

### **Molecular biology**

Constructs of  $\alpha_{1D}$  (AF370009.1),  $\alpha_{1C}$  (NM\_199460.3),  $\alpha_{1F}$  (NP005174) and  $\alpha_{1S}$  (XM\_983862.1) were generously provided by the groups of D. Yue, K. Beam, J. McRory & T. Snutch and J. Streissnig. For Ca<sub>v</sub>1.3 chimeric channels,  $\alpha_{1D}E29_{1S}$ ,  $\alpha_{1D}E33_{1C}$ ,  $\alpha_{1D}E32_{1D}$ ,  $\alpha_{1D}E32_{1F}$  or  $\alpha_{1D}E32_{1D\Delta}6His$  were generated by using overlap extension PCR to fuse different exons: exon 29 from Ca<sub>v</sub>1.1 channel, exon 33 from Ca<sub>v</sub>1.2 channel, exon 32 from Ca<sub>v</sub>1.3 channel, exon 32 from Ca<sub>v</sub>1.4 channel or the His-tag (6 histidines) into IVS3-S4 loop of  $\alpha_{1D}E32_{1D\Delta}$ , respectively. For  $\alpha_{1D}E29_{1S}$  and  $\alpha_{1D}E32_{1F}$ , glycine residues substitute for original amino acids within IVS3-S4 loop ( $\alpha_{1D}E29_{1S}HalfG$ ,  $\alpha_{1D}E29_{1S}AllG$ ,  $\alpha_{1D}E32_{1F}HalfG$ ,  $\alpha_{1D}E32_{1F}AllG$ ) by QuikChange Lightning Site-Directed Mutagenesis Kit (Agilent Technologies). After PCR reaction, the segments were digested with 2 unique sites BamHI and KpnI and inserted to replace the previous region. For  $\alpha_{1D\Delta}E32_{1D\Delta}-DCT_F$ , DCT derived from  $\alpha_{1F}$  was amplified by PCR with flanking SpeI and XbaI and fused to mutant  $\alpha_{1D}$  ( $\alpha_{1D\Delta}$ ) with the carboxyl terminal being truncated out. To make construct of  $\alpha_{1D\Delta}E29_{1S}AllG-DCT_F$ , segment from  $\alpha_{1D}E29_{1S}AllG$  was amplified by PCR with flanking BglII and BstEII and cloned directionally via these 2 unique sites into corresponding region of  $\alpha_{1D\Delta}E32_{1D\Delta}-DCT_F$ . For  $\alpha_{1D\Delta}[6His-E29_{1S}AllG-6His]-$

DCT<sub>F</sub>, overlap extension PCR was performed, similar to  $\alpha_{1D}E32_{1D}\Delta 6His$ .

### Transfection of cDNA constructs

HEK293 cells were cultured in 60 mm dishes, and recombinant channels were transiently transfected according to an established calcium phosphate protocol.<sup>24</sup> We applied 5  $\mu$ g of cDNA encoding the desired  $\alpha_1$  subunit, along with 4  $\mu$ g of rat brain  $\beta_{2a}$  (M80545) and 4  $\mu$ g of rat brain  $\alpha_2\delta$  (NM012919.2) subunits. All of the above cDNA constructs were driven by a cytomegalovirus promoter. To enhance expression, cDNA for simian virus 40 T antigen (1–2  $\mu$ g) was also co-transfected. Cells were washed with PBS 6–8 h after transfection and maintained in supplemented DMEM, then incubated for at least 48 h in a water-saturated 5% CO<sub>2</sub> incubator at 37°C before whole-cell recordings.

### Whole-cell electrophysiology

Whole-cell recordings of transfected HEK293 cells were obtained at room temperature (25°C) using an Axopatch 200B amplifier (Axon Instruments). Electrodes were pulled with borosilicate glass capillaries by a programmable puller (P-1000, Sutter Instruments, USA) and heat-polished by a microforge (MF-900, Narishige, Japan), resulting in 1–3 M $\Omega$  resistances, before series resistance compensation of 70% or more. The internal solutions contained, (in mM): CsMeSO<sub>3</sub>, 135; CsCl<sub>2</sub>, 5; MgCl<sub>2</sub>, 1; MgATP, 4; HEPES, 5; and EGTA, 5; at 290 mOsm adjusted with glucose and at pH 7.3 adjusted with CsOH. The bath solution contained (in mM): TEA-MeSO<sub>3</sub>, 140; HEPES, 10; BaCl<sub>2</sub>, 10; 300 mOsm, adjusted with glucose and at pH 7.3 adjusted with TEAOH, all according to the previous report.<sup>24</sup>

### Antibody incubation of live cells

HEK293 cells transfected with desired recombinant channels were washed with Tyrode solution contained, (in mM): NaCl, 129; KCl, 5; CaCl<sub>2</sub>, 2; MgCl<sub>2</sub>, 1; glucose, 30; Hepes, 25; 300 mOsm, adjusted with glucose and at pH7.3 adjusted with NaOH at room temperature. Cells were then incubated for 1–2 h in Tyrode solution containing THE<sup>TM</sup> His Tag Antibody, mAb, Mouse (GenScript A00186-100), 1:1000 dilution.

### Immunocytochemistry

HEK293 cells on confocal dishes were rinsed briefly in phosphate-buffered saline (PBS), fixed with ice cold 4 % paraformaldehyde in PBS (pH 7.4) for 20 min at the room temperature, then washed 3 times with ice-cold PBS. Fixed cells were then permeabilized with 0.3% Triton X-100, blocked with 10% normal goat serum in PBS for 1 h at room temperature, and incubated overnight at 4°C in primary antibodies: THE<sup>TM</sup> His Tag Antibody, mAb, Mouse (1:1000 dilution; GenScript). The next day, cells were washed with PBS 3 times, incubated at room temperature for 2 h in a 1:800 dilution of anti-mouse-Alexa 568 (Invitrogen), and washed with PBS 3 times.

### TIRF microscopy

Following immunocytochemistry, fluorescence measurements of HEK293 cells were acquired with Nikon Ti-E automatic inverted microscope (A1RSi) through a 100 $\times$ oil TIRF objective. For Alexa 568 imaging, excitation was delivered by a solid-state laser featuring a 561-nm line. TIRF images were analyzed with Image J and Matlab software.

### Analysis and fitting for channel activation

Voltage-dependent activation of the current was fitted according to Boltzmann equation,

$$n = \frac{1}{1 + e^{-\frac{(V-V_{1/2})}{S}}}$$

where  $n$  is the normalized activation,  $V_{1/2}$  is the  $V_m$  for half-maximal conductance/activation and  $S$  is the slope factor.

The time constant of activation was achieved from the fast activation process of Ba<sup>2+</sup> current  $I_{Ba}$ , by fitting with a single-exponential function,

$$I = I_0 \cdot e^{-t/\tau} + C$$

where  $I_0$  is the amplitude of the current,  $\tau$  is the specific time constant and  $C$  is a constant to compensate leakage current when necessary.

### Data analysis and statistics

Data were analyzed in Matlab and Origin software. Standard error of the mean (SEM) and student  $t$ -test

(2-tailed with criteria of significance: \*,  $p < 0.05$ ; \*\*,  $p < 0.01$  and \*\*\*,  $p < 0.001$ ) were calculated when applicable.

## Abbreviations

CDI  $\text{Ca}^{2+}$ -dependent inactivation  
 DCT distal carboxyl terminus  
 LTCCs L-type  $\text{Ca}^{2+}$  channels  
 VSDs voltage sensing domains

## Disclosure of potential conflicts of interest

No potential conflicts of interest were disclosed.

## Acknowledgments

We thank all Liu-Lab (X-Lab) members for discussions. We acknowledge the researchers who shared constructs as indicated in the Methods section. We also thank Drs. D.T. Yue and M.R. Tadross for providing Matlab-based ZStudio program for whole-cell patch-clamp recording, and Mr. P. Jiang for reprogramming and customizing ZStudio.

## Funding

This work is supported by Natural Science Foundation of China (NSFC) grants 81171382, 31370822 and 81371604; Beijing Natural Science Foundation (BNSF) grant 7142089; and Tsinghua National Lab for Information Science and Technology (TNList) Cross-discipline Foundation. XDL also receives support from Tsinghua-Peking Center for Life Sciences (CLS).

## Author contributions

NL and YXL conducted the experiments; NL and YXY performed the analyses; XDL and NL wrote the paper; XDL designed the experiments and conceived the project.

## References

- [1] Catterall WA. International union of pharmacology. XLVIII. Nomenclature and structure-function relationships of voltage-gated calcium channels. *Pharmacol Rev* 2005; 57:411-25; PMID:16382099; <http://dx.doi.org/10.1124/pr.57.4.5>
- [2] Wu J, Yan Z, Li Z, Yan C, Lu S, Dong M, Yan N. Structure of the voltage-gated calcium channel Cav1.1 complex. *Science* 2015; 350:aad2395-aad; PMID:26680202; <http://dx.doi.org/10.1126/science.aad2395>
- [3] Catterall WA. Structure and regulation of voltage-gated  $\text{Ca}^{2+}$  channels. *Annu Rev Cell Dev Biol* 2000; 16:521-55; PMID:11031246; <http://dx.doi.org/10.1146/annurev.cellbio.16.1.521>
- [4] Tombola F, Pathak MM, Isacoff EY. How does voltage open an ion channel? *Ann Rev Cell Dev Biol* 2006; 22:23-52; PMID:16704338; <http://dx.doi.org/10.1146/annurev.cellbio.21.020404.145837>
- [5] Swartz KJ. Sensing voltage across lipid membranes. *Nature* 2008; 456:891-7; PMID:19092925; <http://dx.doi.org/10.1038/nature07620>
- [6] Xu Y, Ramu Y, Lu Z. A shaker  $\text{K}^{+}$  channel with a miniature engineered voltage sensor. *Cell* 2010; 142:580-9; PMID:20691466; <http://dx.doi.org/10.1016/j.cell.2010.07.013>
- [7] Tuluc P, Yarov-Yarovoy V, Benedetti B, Flucher BE. Molecular interactions in the voltage sensor controlling gating properties of  $\text{Ca}_v$  calcium channels. *Structure* 2016; 24:261-71; PMID:26749449; <http://dx.doi.org/10.1016/j.str.2015.11.011>
- [8] Mathur R, Zheng J, Yan Y, Sigworth FJ. Role of the S3-S4 linker in Shaker potassium channel activation. *J Gen Physiol* 1997; 109:191-9; PMID:9041448; <http://dx.doi.org/10.1085/jgp.109.2.191>
- [9] Bezanilla F. Voltage sensor movements. *J Gen Physiol* 2002; 120:465-73; PMID:12356849; <http://dx.doi.org/10.1085/jgp.20028660>
- [10] Tuluc P, Benedetti B, Coste de Bagnaux P, Grabner M, Flucher BE. Two distinct voltage-sensing domains control voltage sensitivity and kinetics of current activation in  $\text{Ca}_v1.1$  calcium channels. *J Gen Physiol* 2016; 147:437-49; PMID:27185857; <http://dx.doi.org/10.1085/jgp.201611568>
- [11] Xu W, Lipscombe D. Neuronal  $\text{Ca}_v1.3\alpha1$  L-type channels activate at relatively hyperpolarized membrane potentials and are incompletely inhibited by dihydropyridines. *J Neurosci* 2001; 16:5944-51.
- [12] Tang ZZ, Liang MC, Lu S, Yu D, Yu CY, Yue DT, Soong TW. Transcript scanning reveals novel and extensive splice variations in human L-type voltage-gated calcium channel,  $\text{Cav}1.2 \alpha1$  subunit. *J Biol Chem* 2004; 279:44335-43; PMID:15299022; <http://dx.doi.org/10.1074/jbc.M407023200>
- [13] Lin Z, Lin Y, Schorge S, Pan JQ, Beierlein M, Lipscombe D. Alternative splicing of a short cassette exon in  $\alpha1B$  generates functionally distinct N-type calcium channels in central and peripheral neurons. *J Neurosci* 1999; 13:5322-31; PMID:10377343
- [14] Hans M, Urrutia A, Deal C, Brust PF, Stauderman K, Ellis SB, Harpold MM, Johnson EC, Williams ME. Structural elements in domain IV that influence biophysical and pharmacological properties of human  $\alpha1A$ -containing high-voltage-activated calcium channels. *Biophys J* 1999; 76:1384-400; PMID:10049321; [http://dx.doi.org/10.1016/S0006-3495\(99\)77300-5](http://dx.doi.org/10.1016/S0006-3495(99)77300-5)
- [15] Bourinet E, Soong TW, Sutton K, Slaymaker S, Mathews E, Monteil A, Zamponi GW, Nargeot J, Snutch TP. Splicing of alpha 1A subunit gene generates phenotypic variants of P- and Q-type calcium channels. *Nat Neurosci* 1999; 2:407-15; PMID:10321243; <http://dx.doi.org/10.1038/8070>
- [16] Adams PJ, Ben-Johny M, Dick IE, Inoue T, Yue DT. Apocalmodulin itself promotes ion channel opening and  $\text{Ca}^{2+}$

- regulation. *Cell* 2014; 159:608-22; PMID:25417111; <http://dx.doi.org/10.1016/j.cell.2014.09.047>
- [17] Tuluc P, Molenda N, Schlick B, Obermair GJ, Flucher BE, Jurkat-Rott K. A CaV1.1 Ca<sup>2+</sup> channel splice variant with high conductance and voltage-sensitivity alters EC coupling in developing skeletal muscle. *Biophys J* 2009; 96:35-44; PMID:19134469; <http://dx.doi.org/10.1016/j.bpj.2008.09.027>
- [18] Tang ZZ, Zheng S, Nikolic J, Black DL. Developmental control of CaV1.2 L-type calcium channel splicing by fox proteins. *Mol Cell Biol* 2009; 29:4757-65; PMID:19564422; <http://dx.doi.org/10.1128/MCB.00608-09>
- [19] Tan GMY, Yu D, Wang J, Soong TW. Alternative splicing at C terminus of CaV1.4 calcium channel modulates calcium-dependent inactivation, activation potential, and current density. *J Biol Chem* 2012; 287:832-47; PMID:22069316; <http://dx.doi.org/10.1074/jbc.M111.268722>
- [20] Safa P, Boulter J, Hales TG. Functional properties of CaV1.3 ( $\alpha$ 1D) L-type Ca<sup>2+</sup> Channel Splice Variants Expressed by Rat Brain and Neuroendocrine GH3 Cells. *J Biol Chem* 2001; 276:38727-37; PMID:11514547; <http://dx.doi.org/10.1074/jbc.M103724200>
- [21] McRory JE. The CACNA1F gene encodes an L-type calcium channel with unique biophysical properties and tissue distribution. *J Neurosci* 2004; 24:1707-18; PMID:14973233; <http://dx.doi.org/10.1523/JNEUROSCI.4846-03.2004>
- [22] Mori MX, Erickson MG, Yue DT. Functional stoichiometry and local enrichment of calmodulin interacting with Ca<sup>2+</sup> channels. *Science* 2004; 304:432-5; PMID:15087548; <http://dx.doi.org/10.1126/science.1093490>
- [23] Xu S-Z, Zeng F, Lei M, Li J, Gao B, Xiong C, et al. Generation of functional ion-channel tools by E3 targeting. *Nat Biotechnol* 2005; 23:1289-93; PMID:16170312; <http://dx.doi.org/10.1038/nbt1148>
- [24] Liu X, Yang PS, Yang W, Yue DT. Enzyme-inhibitor-like tuning of Ca<sup>2+</sup> channel connectivity with calmodulin. *Nature* 2010; 463:968-72; PMID:20139964; <http://dx.doi.org/10.1038/nature08766>
- [25] Nakai J, Adams BA, Imoto K, Beam KG. Critical roles of the S3 segment and S3-S4 linker of repeat I in activation of L-type calcium channels. *Proc Natl Acad Sci U S A* 1994; 91:1014-8; PMID:8302825; <http://dx.doi.org/10.1073/pnas.91.3.1014>